Design of solar cells coupled to resonant multi-dielectric structures : Effect of doping on conversion efficiency

Césaire Ngor Ndiaye, Abdoulaye Sène, Modou Kara Mbengue et Lamine Thiaw
Ecole Supérieure Polytechnique de Dakar, Université Cheikh Anta Diop de Dakar, SENEGAL
cesairengor.ndiaye@esp.sn
abdoulaye37.sene@ucad.edu.sn
modoukara1.mbengue@ucad.edu.sn
lamine.thiaw@ucad.edu.sn

Abstract*— Despite years of efforts to improve the conversion efficiency of photovoltaic solar cells, the latter is still below expectations in relation to the solar potential available on the earth's surface. Since the production of electricity by solar cells is intimately linked to the amount of light captured by these cells, the use of materials capable of absorbing almost the entire solar spectrum, and light trapping, play a key role. As a result, III-V materials and their ternary and quaternary alloys have been the most widely used semiconductors in optoelectronics in recent years. Among these materials, indium gallium nitride (In.Ga.N) has been an undeniable advantage for photovoltaics for the past ten years, thanks to its scalable energy gap that sweeps the entire visible spectrum, from the near infrared (InN gap = 0.7eV) to the ultraviolet (GaN gap = 3.4eV). In addition, a synthesis method based on complex admittances has been implemented in our previous work to improve conversion efficiency. In this context, this work focuses on the use of the In.Ga.N alloy to model a nanostructured thin-film mono-junction solar cell and determine its electrical performance using Matlab/Simulink software under illumination with the AM1.5G spectrum in the static regime after its coupling with the resonant multi-dielectric structure. To obtain more accurate results, optical properties and physical models such as recombination, doping and the temperature-dependent mobility model were taken into account in the simulations. The results of the study show that the best electrical parameters for the optimized coupled cell are as follows : $J_{sc} = 36.62 mA/cm^2$, $V_{oc} = 0.9569\ V$ et $\eta = 33.50\%$. Compared with control cell ($J_{sc} = 32.67 mA/cm^2$, $V_{oc} = 0.94V$ et $\eta = 26.50\%$), this shows that the results obtained are promising.

***Keywords*— Nanostructures, solar cell, coupling, sizing, recombination, doping, mobility, multi-dielectric, $In_xGa_{1-x}N$, static regime, multi-spectral illumination, resonant structure.**

I. INTRODUCTION

Today, energy in general, and electricity in particular, underpins all human activity, and is the lifeblood of the modern economy. In view of the current problems linked to the depletion of fossil energy reserves (coal, oil, gas, uranium, etc.) and the environmental risks associated with greenhouse gas emissions leading to global warming, future energy management is at the heart of current affairs. To deal with this situation, renewable energies are an unavoidable alternative in the global energy crisis. One of the most widely used and non-polluting renewable energies is solar power, due to its availability and inexhaustible supply [1], [2]. However, its conversion efficiency is still below expectations. As a result, improving the efficiency of these devices is a major challenge if we are to make the most of this clean, renewable energy source. That's why researchers and engineers are constantly pushing back the limits of solar efficiency, paving the way for a more sustainable future less dependent on fossil fuels [3].

On the one hand, in order to improve this performance, several optimization techniques such as doping [1], the non-linearity [2-4], the use of ferromagnetic materials [4] and various light trapping strategies to improve optical absorption have been implemented [5]. It is within this framework that a synthesis method based on complex admittances, widely used to synthesize optical functions, has been implemented in our previous work [6]. The results of this work have shown that it is possible to obtain total absorption and therefore amplification of the optical field ($10\text{-}10^4$) with extreme sensitivity to illumination conditions in nanostructured multi-dielectric thin-film stacks [7], [8], [9].

In addition, a review of the performance of various thin-film photovoltaic solar cell technologies enabled us to justify our choice of a mono-junction cell based on Indium Gallium Nitride (In.Ga.N), a III-V family material with attractive properties for optoelectronic applications, particularly photovoltaics. These properties include a gap that can be adjusted according to the indium composition, enabling the formation of alloys with bandgap energies

ISSN: 2961-6603

covering virtually the entire spectrum (from 0.7eV to 3.42eV), high radiation tolerance, high mobility and a high absorption coefficient. These properties include a gap that can be adjusted according to the indium composition, enabling the formation of alloys with bandgap energies covering virtually the entire spectrum (from 0.7eV to 3.42eV), high radiation tolerance, high mobility and a high absorption coefficient [10].

Most work on single-junction solar cells based on Indium Gallium Nitride (In.Ga.N) was based on the random allocation of a fraction of indium, to deduce the cell's optimum efficiency. Motivated by the same objective, we plan to optimize the performance of this type of solar cell by adjusting the incident power as well as the doping of the layers. It is in this context that the present work focuses on the modeling and simulation of this mono-junction solar cell coupled to dielectric nanostructures exalting the optical field under multi-spectral illumination in the static regime.

II. SYNTHESIS METHOD

To synthesize such resonant structures, alternating low-index dielectric thin films are used (SiO_2) and high index (Ta_2O_5) placed between a superstrate (Verre : BK7) and a substrate (air) is illuminated by an obliquely incident light source, as shown in the Fig. 1.

A. Calculation of stack absorption

Our aim is to have a total absorption that can be calculated directly from the following energy balance relationship [11], [12] :

$$A + R + D + T = 100\% \quad (1)$$

Where A, R, T and D represent absorption, reflection, transmission and scattering respectively.

In an energy balance, what is absorbed (A), reflected (R), transmitted (T) and scattered (D) must be equal to the incident field. In our case, scattering is zero because we are considering perfectly smooth surfaces, and transmission is also zero because we are working under conditions of total reflection ; this reduces the expression (1) to : $A = 1 - R$. So, to have 100% absorption in the stack, the reflection must be zero. In thin-film theory, the intensity reflection coefficient R is defined as the ratio between the reflected flux Φ_0^- and incident flow Φ_0^+ :

$$R = |r|^2 = \left|\frac{\tilde{n}_0 - Y_0}{\tilde{n}_0 + Y_0}\right|^2 \quad (2)$$

With :

$\tilde{n}_0$: effective index at interface 0 ;

$\vec{E}_{tg,0}^-$: tangential component of the electric field reflected at the interface 0 ;

$\vec{E}_{tg,0}^+$: tangential component of the electric field incident at the interface 0 ;

Y_0 : complex stack admittance ;

r : amplitude reflection coefficient.

So, from this expression, to cancel out this reflection, which is synonymous with total absorption, it is necessary that Y_0 is equal to $\tilde{n}_0$. To do this, we use the recurrence relation between complex admittances (3) obtained from the transition matrix (4) to go from Y_p to Y_0.

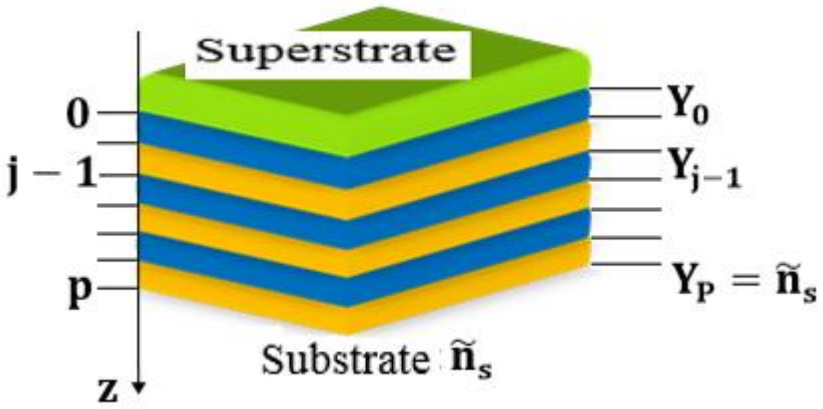

Fig. 1 Admittance Y_0 deduced by recurrence from initial substrate admittance $Y_p = \tilde{n}_s$

ISSN: 2961-6603

$$Y_{j-1} = \frac{Y_j \cos(\delta_j) - i\tilde{n}_j \sin(\delta_j)}{\cos(\delta_j) - i\frac{Y_j}{\tilde{n}_j}\sin(\delta_j)} \quad (3)$$

$$M_j = \begin{pmatrix} \cos(\delta_j) & -\frac{i}{\tilde{n}_j}\sin(\delta_j) \\ -i\tilde{n}_j \sin(\delta_j) & \cos(\delta_j) \end{pmatrix} \quad (4)$$

Preliminary results obtained by plotting the evolution of absorption as a function of illumination wavelength show a resonance centered at 532 nm, as indicated by the Fig. 2.

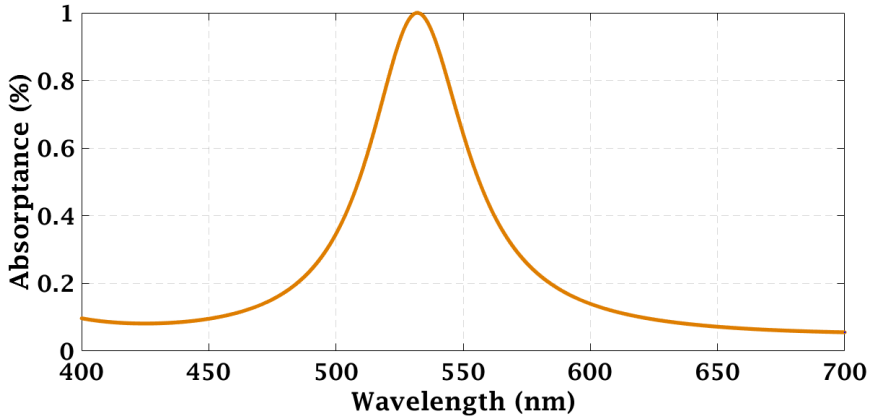

Fig. 2 Evolution of absorption as a function of wavelength

Remember that this resonance is strongly related to the amplification of the optical field in the stack, and the narrower the spectral band of the absorption profile, the higher the field.

B. Stationary field distribution in the stack

To show the effect of resonance on field amplification in the stack, we always use the matrix relationship (4). Since the admittances are known at the various diopters, we can relate the fields to the interfaces using this matrix relationship (4). Thus, in the case of the electric field, we have :

$$\vec{z} \wedge \vec{E}_{tg,j-1} = \cos\delta_j \, (\vec{z} \wedge \vec{E}_{tg,j}) \; - \frac{i}{\tilde{n}_j}\sin\delta_j \, \vec{H}_{tg,j} \quad (5)$$

$$\text{Or} \qquad \vec{H}_{tg,j} = Y_j \vec{z} \wedge \vec{E}_{tg,j} \quad (6)$$

This implies that :

$$\vec{z} \wedge \vec{E}_{tg,j-1} = \cos\delta_j \left(\vec{z} \wedge \vec{E}_{tg,j}\right) - i\frac{Y_j}{\tilde{n}_j}\sin\delta_j \, (\vec{z} \wedge \vec{E}_{tg,j}) \quad (7)$$

So, simplifying expression (7), we obtain the following relationship :

$$\vec{E}_{tg,j-1} = \left[\cos\delta_j - \, i\frac{Y_j}{\tilde{n}_j}\sin\delta_j\right]\vec{E}_{tg,j} \quad (8)$$

From relationship (8), we can determine the values of the electromagnetic field in the entire stack from the known admittances in each layer of the stack, as shown in this map in Fig. 3.

ISSN: 2961-6603

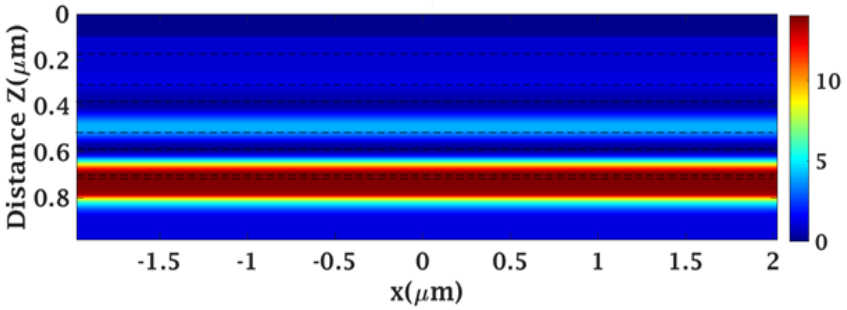

Fig. 3 Field mapping in the stack

In this figure, over-intensification increases to 14 in the last layer of the stack. It's worth noting that this amplified field will play an important role in improving the efficiency of the coupling between this resonant structure and the solar cell. However, to get the best out of the latter, it is necessary to make an optimal choice of the material to be used.

III. SOLAR CELL MODELING

To improve the performance of a solar cell, we can act on its structure.

A. *Description of the solar cell*

The cell studied is a single-junction thin-film cell based on $In_xGa_{1-x}N$. It comprises four essential parts (Fig. 4) :

- An anti-reflective coating to reduce light reflection on the front face, one of the main sources of losses that limit the conversion efficiency of solar cells.
- A front layer, also known as the emitter or P-doped front layer ;
- An N-doped layer, also called base ;
- And finally, between the P-doped layer and the N-doped layer, there's the junction or space charge zone, which separates the electron-hole pairs thanks to the prevailing electric field. It lies between z_j et $z_j + w$ where w is the width of this zone [13].

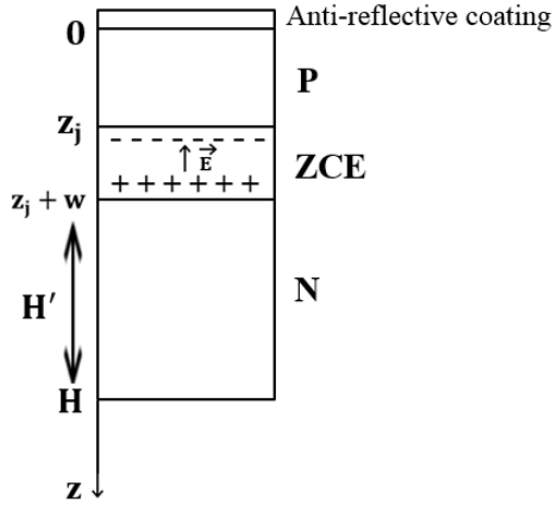

Fig. a Theoretical model

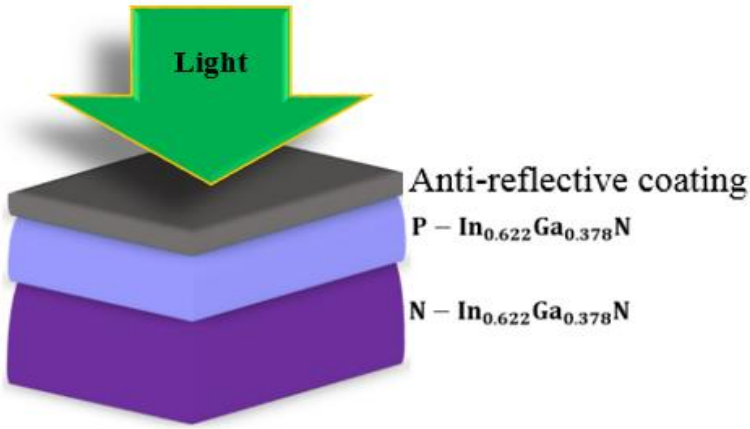

Fig. b Real structure

Fig. 4 $In_xGa_{1-x}N$-based single-junction solar cells [14]

This choice is based on its wide direct gap covering virtually the entire solar spectrum from ultraviolet to near infrared simply by changing the Indium composition, its good resistance to high temperatures and high powers, its strong interatomic bonds, its high thermal conductivity and its high absorption coefficient of the order of $10^5 cm^{-1}$.

B. *Photocurrent density $J_{ph}(\lambda)$*

The cell is modeled in the static regime under multi-spectral illumination where the photocurrent for a wavelength ($J_{ph}(\lambda)$) is obtained by the contribution of three current densities J_n , J_p et J_{ZCE} whose expressions are as follows: :

ISSN: 2961-6603

$$J_n(\lambda) = \left[\frac{qF(1-R)\alpha L_n}{\alpha^2 {L_n}^2 - 1}\right]\left[\frac{\left(\frac{S_n L_n}{D_n}+\alpha L_n\right) - e^{-\alpha z_j}\left(\left(\frac{S_n L_n}{D_n}\right)\cosh\left(\frac{z_j}{L_n}\right)+\sinh\left(\frac{z_j}{L_n}\right)\right)}{\left(\frac{S_n L_n}{D_n}\right)\sinh\left(\frac{z_j}{L_n}\right)+\cosh\left(\frac{z_j}{L_n}\right)} - \alpha L_n e^{-\alpha x_j}\right] \quad (9)$$

$$J_p(\lambda) = \left[\frac{qF(1-R)\alpha L_p}{\alpha^2 {L_p}^2 - 1}\right] e^{-\alpha(z_j+w)}\left\{\alpha L_p - \frac{\left(\frac{S_p L_p}{D_p}\right)\left[\cosh\left(\frac{H'}{L_p}\right) - e^{-\alpha H'}\right]+\sinh\left(\frac{H'}{L_p}\right)+\alpha L_p e^{-\alpha H'}}{\left(\frac{S_p L_p}{D_p}\right)\sinh\left(\frac{H'}{L_p}\right)+\cosh\left(\frac{H'}{L_p}\right)}\right\} \quad (10)$$

$$J_{ZCE}(\lambda) = -q.\emptyset(1-R).e^{-\alpha.z_j}(1-e^{-\alpha w}) \quad (11)$$

With

- $J_n(\lambda)$: contribution of the emitter to the total photocurrent for a given wavelength.
- $J_p(\lambda)$: contribution of the base to the total photocurrent for a given wavelength.
- $J_{ZCE}(\lambda)$: contribution of the space charge zone to the total photocurrent for a given wavelength.

Consequently, the photo-current density $J_{ph}(\lambda)$ by incident radiation wavelength is the sum of the currents in the three zones:

$$J_{ph}(\lambda) = J_n(\lambda) + J_p(\lambda) + J_{ZCE}(\lambda) \quad (12)$$

The total photo-current density J_{ph} is obtained by integrating the current density $J_{ph}(\lambda)$ over the entire solar spectrum used. Its expression is given by the following relationship :

$$J_{ph} = \int_{\lambda_{min}}^{\lambda_{max}} J_{ph}(\lambda)d\lambda = \int_{\lambda_{min}}^{\lambda_{max}} J_n(\lambda)d\lambda + \int_{\lambda_{min}}^{\lambda_{max}} J_p(\lambda)d\lambda + \int_{\lambda_{min}}^{\lambda_{max}} J_{ZCE}(\lambda)d\lambda \quad (13)$$

C. Characteristic values of the solar cell

Carrier and current densities can be obtained analytically to determine the current-voltage (J-V) characteristic of p-n junction solar cells. From this main characteristic of the cell, we can see that the behavior of a solar cell can be studied through four main physical quantities : short-circuit current density (J_{sc}), open-circuit voltage (V_{oc}), maximum voltage (V_m) and maximum current density (J_m). Thus, based on the ideal one-diode model, the total current density, J, in p-n junction solar cells can be expressed as follows [15], [16], [17] :

$$J = J_{ph} - J_{obsc} = J_{ph} - J_0\left(e^{\frac{qV}{K_B T}} - 1\right) \quad (14)$$

With :

- J_{ph} : photo-generated current [A]
- J_{obsc} : diode current in darkness [A]
- $J_0 = qn_i^2\left(\frac{D_p}{L_p N_d} + \frac{D_n}{L_n N_a}\right)$: diode saturation current [A]
- D_n et D_p : diffusion coefficients of minority carriers in the P and N zones respectively [$cm^2.s^{-1}$]
- L_n et L_p : scattering lengths in the P and N layers respectively [cm]
- N_d et N_a : doping rate in N and P materials [cm^{-3}]
- $q = 1.602\ 10^{-19}C$: elementary charge of an electron
- V : diode terminal voltage [V]
- $K_B = 1.38\ 10^{-23}\ {}^{J}/_{K}$: Boltzmann constant
- T : temperature in Kelvin

The important physical quantities of a solar cell derive from its current-voltage (J-V) characteristic:

1) *Short-circuit current density J_{sc} :* The short-circuit current in mA (or short-circuit current density in $mA.cm^{-2}$) is the current that flows through the photovoltaic cell when it is short-circuited, i.e. when the voltage at its terminals is zero.

In the ideal case, it merges with the photocurrent density J_{ph} **:**

$$J_{sc} = J_{ph} \quad (15)$$

2) *La tension de circuit ouvert V_{oc}*: is the voltage measured across the cell when it delivers zero current. It is given by the relationship below :

$$V_{oc} = \frac{K_B T}{q}\ln\left(\frac{J_{cc}}{J_0} + 1\right) \quad (16)$$

ISSN: 2961-6603

3) *Le point de puissance maximale :* the maximum power of an illuminated photovoltaic cell is the essential parameter for assessing its performance ; it is given by the relationship :

$$P_m = V_m * J_m \quad (17)$$

4) *Le facteur de forme (FF) :* It's a parameter between 0 and 1, but generally takes values between 0.6 and 0.85, and qualifies the more or less rectangular shape of the solar cell's (J-V) characteristic.

It is defined as the ratio between the maximum power P_m and the product $Jsc * Vco$ according to the following relation :

$$FF = \frac{P_m}{J_{cc}V_{oc}} = \frac{J_m V_m}{J_{cc}V_{oc}} \quad (18)$$

5) *Le rendement de conversion :* The reference parameter for assessing the quality of a solar cell is the conversion efficiency (η). It reflects a PV cell's ability to convert photon energy into electricity. It is defined as the ratio between the maximum power delivered by the cell and the incident solar radiation power P_{inc} [18]. Its expression combines the four characteristic quantities mentioned above and is given by :

$$\eta = \frac{P_m}{P_{inc}} = \frac{J_m * V_m}{P_{inc}} = \frac{FF * J_{cc} * V_{oc}}{S * E} \quad (19)$$

With S the cell surface area of 0.0624 cm^2 and E the illuminance or irradiance in $W.m^{-2}$.

IV. SOLAR CELL/RESONANT STRUCTURE COUPLING

In this section, we will study the effect of coupling the resonant structure to the single-junction solar cell. The aim is to gather as much energy as possible from the resonant structure, in order to optimally excite the solar cell.

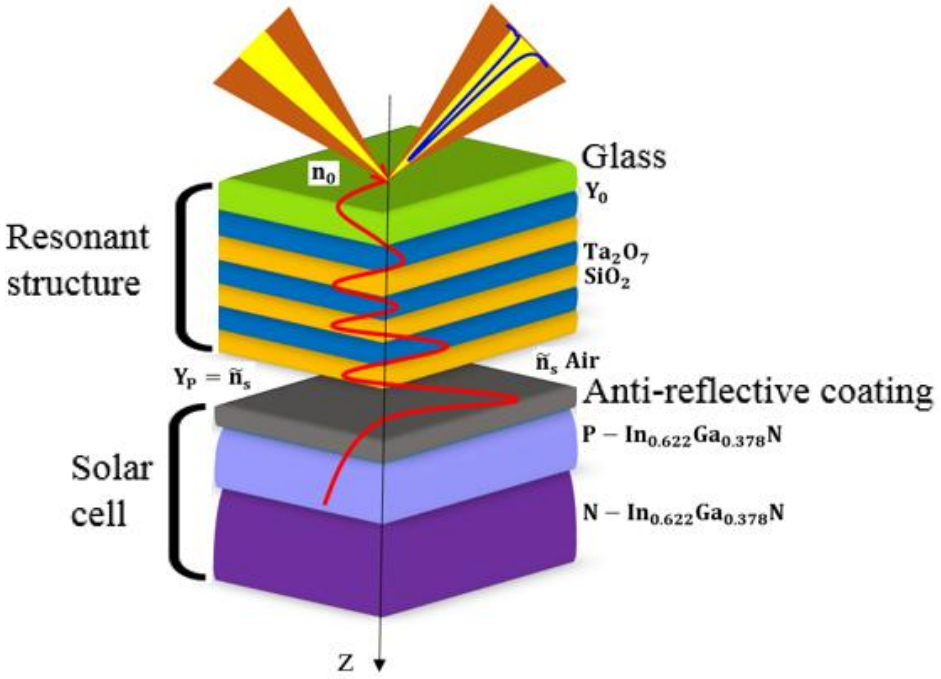

Fig. 5 Single-junction cell coupled with resonant structure

Given the evanescence of the field at the substrate, the solar cell would be brought as close as possible to the resonant multi-dielectric stack until the gap is almost zero, in order to take better advantage of the superintensification. Fig. 6 shows the evolution of absorption as a function of wavelength at zero gap.

ISSN: 2961-6603

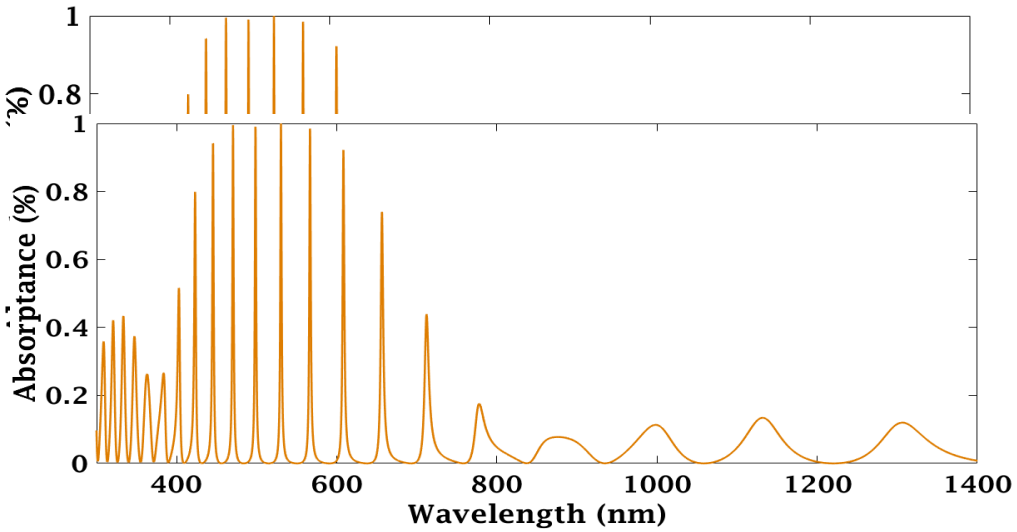

Fig. 6 Evolution of absorption in the coupled solar cell

From this figure, we can clearly see that all wavelengths around 500nm have more than 80% absorption, resulting in field enhancement around these wavelengths. However, the other wavelengths will reach the cell naturally. Representing the evolution of the associated electric field when the conditions for total absorption are met, we obtain Fig. 7 below.

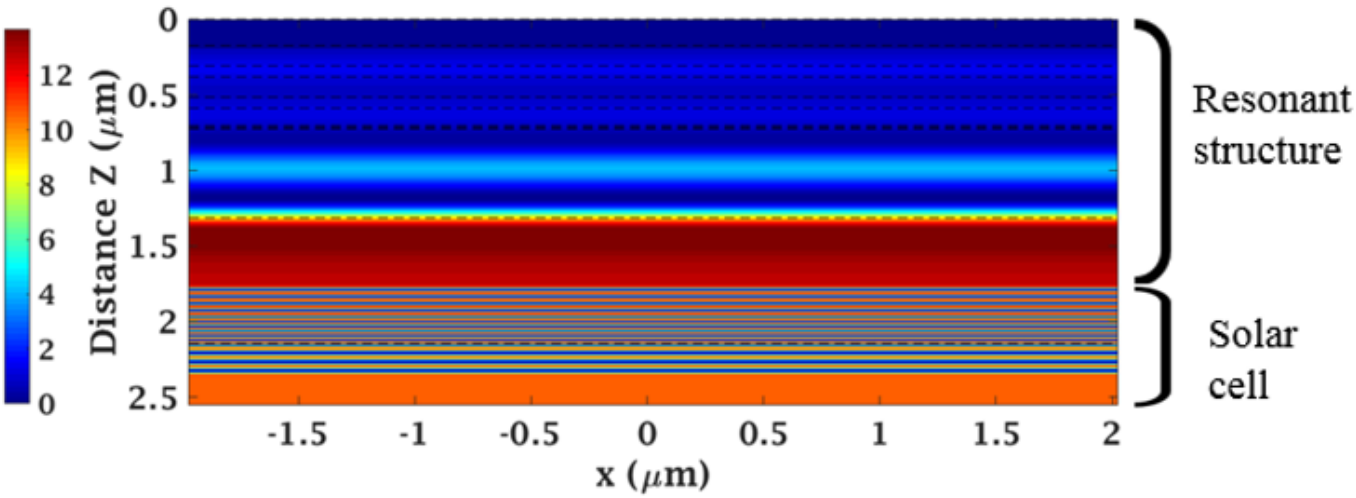

Fig. 7 Field mapping in the coupled solar cell

In this figure, the exaltation of the field in the coupled cell is of the order of 12.

V. Simulation Results and Discussion

Numerical simulation is an important technique used today to determine the performance of photovoltaic solar cells, based on the intrinsic properties of the materials that make them up. This simulation is used to calculate photovoltaic parameters such as short-circuit current density (J_{sc}), open-circuit voltage (V_{oc}), form factor (FF), maximum power (P_{max}) and photovoltaic conversion efficiency.

A. Simulation parameters

The material used in our work $In_xGa_{1-x}N$ (with x the indium composition in the alloy) is defined on the basis of parameters taken from the literature. The lifetimes of minority carriers in Gallium Nitride (GaN) and Indium Nitride (InN) are 6.5 ns and 5.4 ns respectively. [19]. As a result, the carrier lifetimes in the alloy ($In_xGa_{1-x}N$) will be shorter due to fluctuating indium composition [20]. Based on this data, we have assumed a lifetime equal to 1 ns for both holes and electrons, to obtain a much more realistic device. The values of these parameters are shown in Table I below.

ISSN: 2961-6603

TABLEAU I INITIAL PARAMETERS USED IN THE 300 K SIMULATION FOR X = 0.622

Parameters	Expressions	Values	References
Forbidden strip $\boldsymbol{Eg}$ (eV)	$0.7x + 3.42(1-x) - 1.43x(1-x)$	1.39	[17], [21]
Relative Permittivity ε	$15.3x + 8.9(1-x)$	12.88	[22]
Electronic affinity χ (eV)	$4.1 + 0.7(3.42 - E_g)$	5.52	[23], [16]
Density of state in the conduction band N_C ($10^{18}cm^{-3}$)	$0.9x + 2.3(1-x)$	1.43	[22], [15]
Density of state in the valence band N_V ($10^{19}cm^{-3}$)	$5.3x + 1.8(1-x)$	3.98	[15]
Electron and hole lifetime τ_n et τ_p (ns)	$\tau_n = \tau_p$	1	[14], [16]
Surface recombination velocity S_n et S_p ($cm.s^{-1}$)	$S_n = S_p$	1000	[10], [23]
P-layer doping (cm^{-3})	– –	$1.5\ 10^{18}$	[14]
N-layer doping (cm^{-3})	– –	$5\ 10^{17}$	
Layer thickness P (nm)	– –	250	
Layer thickness N (nm)	– –	1000	

Based on these initial parameters, we first simulated the current-voltage I(V) and power-voltage P(V) characteristics of the control cell, and the results obtained are shown in Fig. 8 and Fig. 9 respectively.

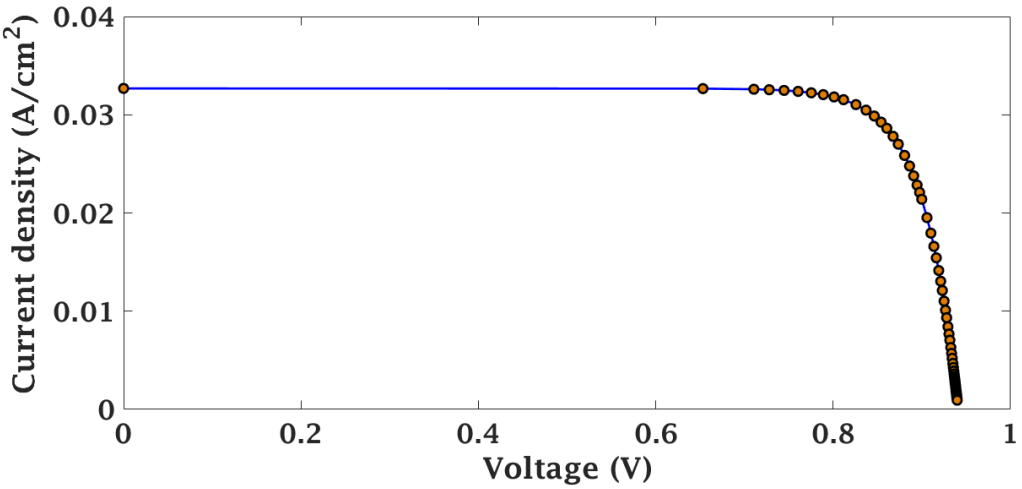

Fig. 8 Current-voltage characteristic of control cell

ISSN: 2961-6603

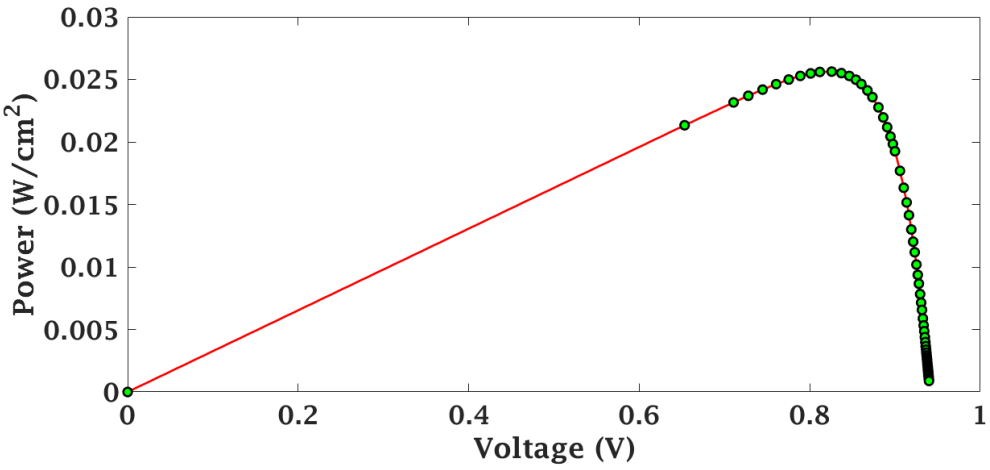

Fig. 9 Control cell power-voltage characteristic

These two curves show that the control cell has an open-circuit voltage $V_{oc} = 0.94$ V et une densité de courant de court-circuit and a short-circuit current density $J_{sc} = 32.67\ mA.cm^{-2}$ i.e. a maximum power of $26.50\ mW.cm^{-2}$.

In order to demonstrate the importance of adding the resonant structure to a conventional solar cell taken as a reference, we simulated the I(V) and P(V) characteristics of the coupled cell shown in Fig. 10 and Fig. 11 respectively.

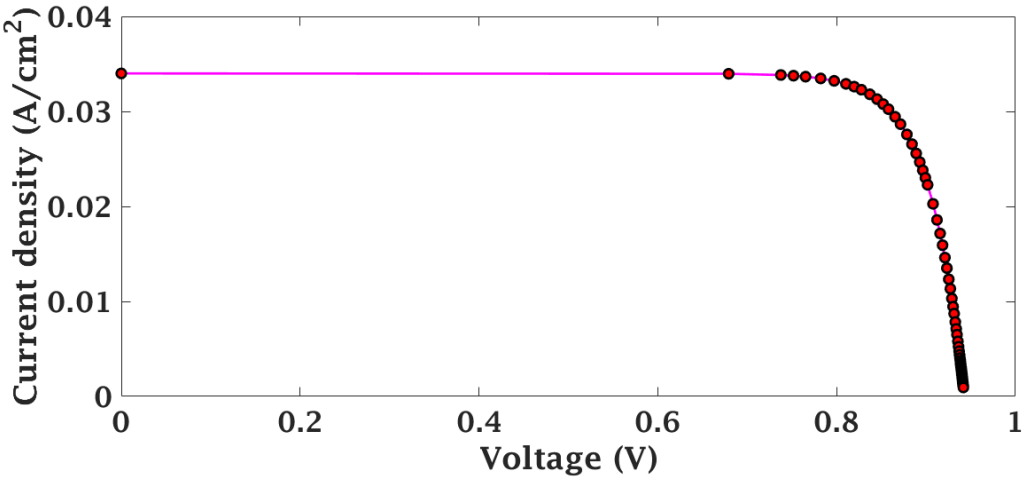

Fig. 10 Current-voltage characteristic of coupled cell

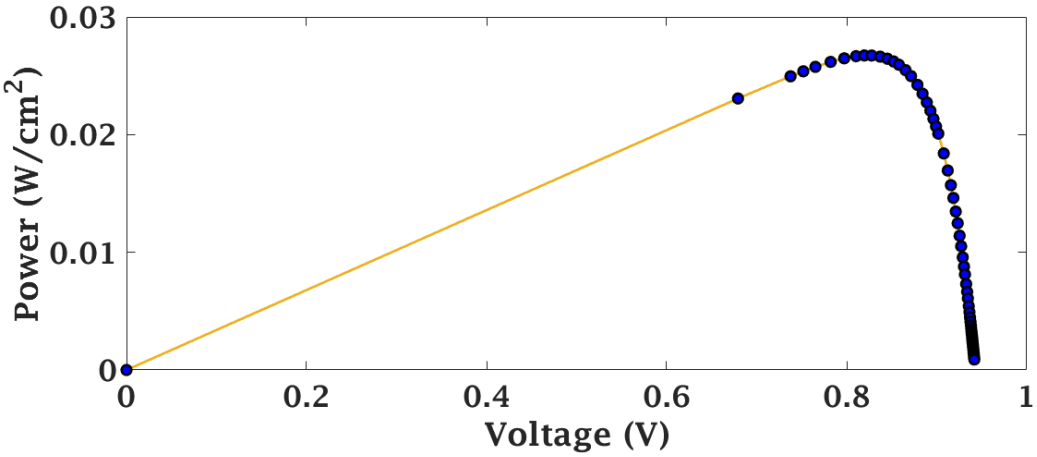

Fig. 11 Power-voltage characteristic of coupled cell

These results show that the coupled cell has an open-circuit voltage $V_{oc} = 0.9428$ V and a short-circuit current density $J_{sc} = 34\ mA.cm^{-2}$ with a maximum power of $26.73\ mW.cm^{-2}$.

Finally, after these two simulations, we turn to a comparative study of these two cells by plotting their I(V) and P(V) characteristics, shown in Fig. 12 and Fig. 13 respectively.

ISSN: 2961-6603

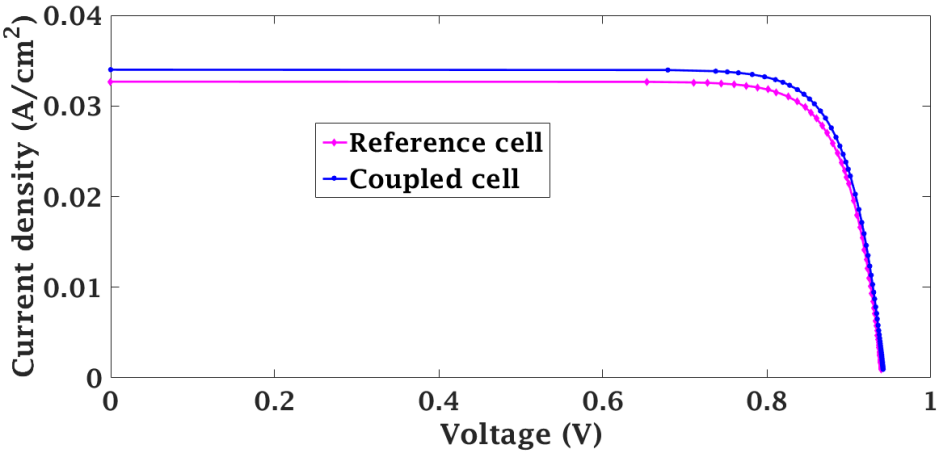

Fig. 12 Current-voltage characteristic of control cell and coupled cell

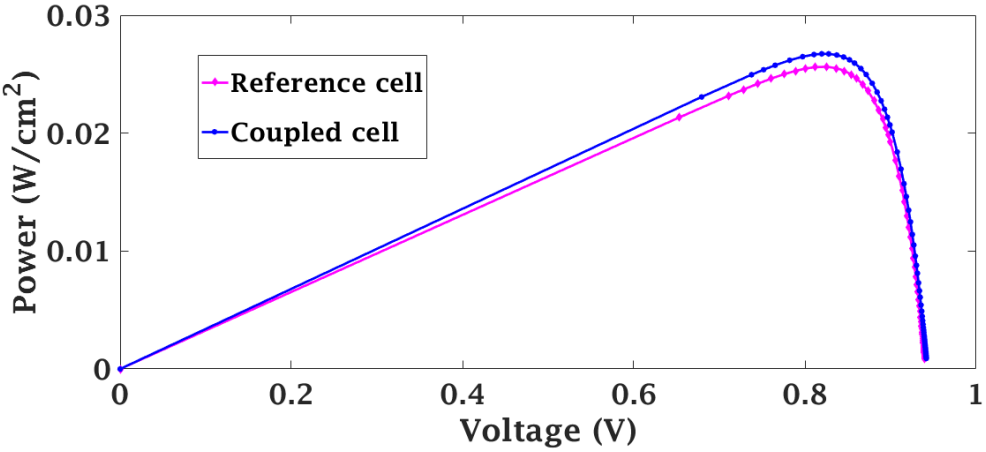

Fig. 13 Power-voltage characteristics of control cell and coupled cell

The various output parameters of these two cells are summarized in Table II below.

TABLEAU II OUTPUT PARAMETERS FOR CONTROL CELL AND COUPLED CELL

	Jsc (mA/cm^2)	**Vco (V)**	**Jmax (mA/cm^2)**	**Vmax (V)**	**Pmax (mW/cm^2)**	**Ƞ (%)**
Reference cell	32.67	0.94	31.53	0.81	26.51	26.50
Coupled cell	34	0.9428	32.61	0.8196	26.73	28.07

From this table, we can observe an increase in short-circuit current density J_{sc} and consequently in conversion efficiency Ƞ. With the addition of the resonant structure; we increase the short-circuit current density J_{sc} from 32.67 mA. cm^{-2} to 34 mA. cm^{-2} and the conversion efficiency from 26.50 % to 28.07 % ; showing the importance of adding the resonant multi-dielectric structure on the performance of the coupled cell compared to the control cell.

B. Optimisation : effects of doping on conversion efficiency

In order to determine the optimal values of the photovoltaic parameters, we will investigate the effect of emitter and base doping on the performance of the $In_{0.622}Ga_{0.378}N$ based cell coupled to the resonant multi-dielectric structure, using MATLAB/SIMULINK software.

ISSN: 2961-6603

1) *Effect of emitter doping (Na) on cell electrical parameters*: to study this effect, we varied the doping concentration of the Na acceptor (P layer) from 10^{17} à 10^{19} cm^{-3}, while the emitter thickness z_j, thickness H' and Nd doping of the base (N layer) were fixed. The cell's output parameters (V_{co}, I_{cc} et η) are shown as curves in Fig. 14 and Fig. 15 respectively.

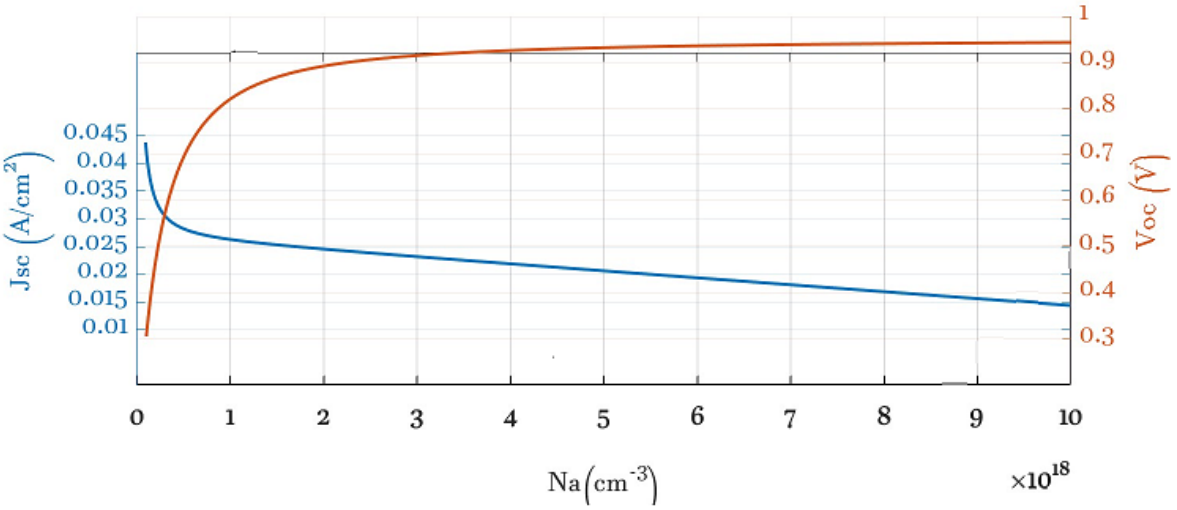

Fig. 14 Short-circuit current density (J_{sc}) and open-circuit voltage (V_{oc}) as a function of Na acceptor doping concentration Na

Fig. 14 illustrates the influence of emitter Na doping on the cell's short-circuit current and open-circuit voltage. According to this figure, the short-circuit current density J_{sc} increases to a value of $43.81\ mA.cm^{-2}$ as the Na doping concentration decreases.

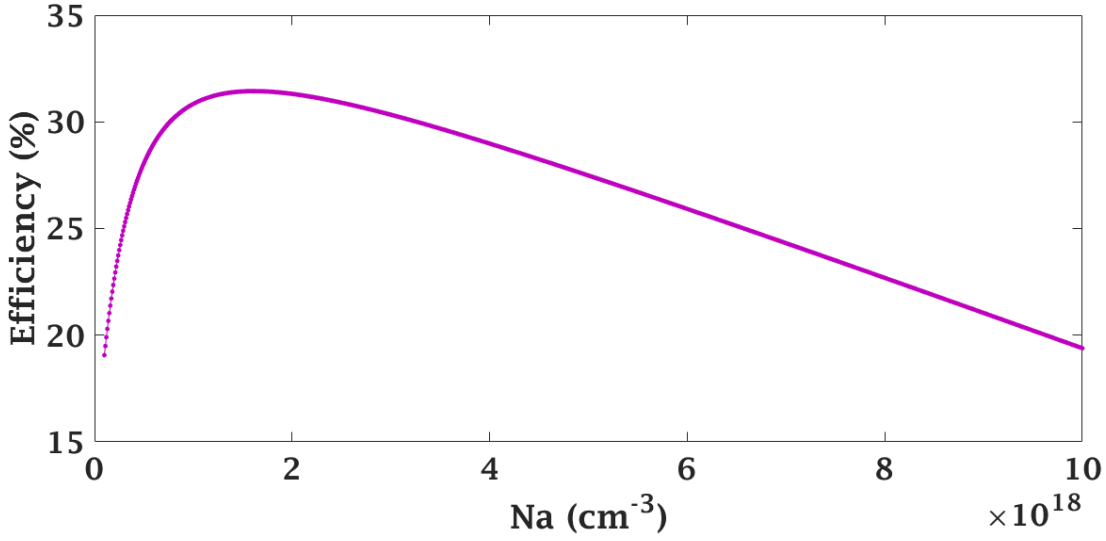

Fig. 15 Solar cell efficiency (η) as a function of Na acceptor doping concentration

From Fig. 15, we can see that as the Na doping concentration increases, the conversion efficiency first increases and then decreases. This is because the conversion efficiency η represents the combined effect of J_{sc} and V_{oc}. Optimum solar cell efficiency is 31.44% (Fig. 15) and is achieved when Na acceptor doping reaches a maximum value of $1.58\ 10^{18}\ cm^{-3}$ and then decreases for higher Na values. This decrease mainly results from the decrease in J_{sc} because after a doping rate of $1.58\ 10^{18}\ cm^{-3}$, the decrease in J_{sc} is greater than the growth in V_{oc}.

2) *Effect of base doping (Nd) on cell electrical parameters*: in this section, we simulate the effect of base doping on solar cell characteristics. As a result, we varied the Nd doping (N layer) from 10^{17} à 10^{18} cm^{-3} while fixing the Na value at $1.58\ 10^{18}\ cm^{-3}$ as well as the emitter and base thickness values. The results obtained (V_{oc}, J_{sc} et η) are shown in Fig. 16 and Fig. 17 respectively.

ISSN: 2961-6603

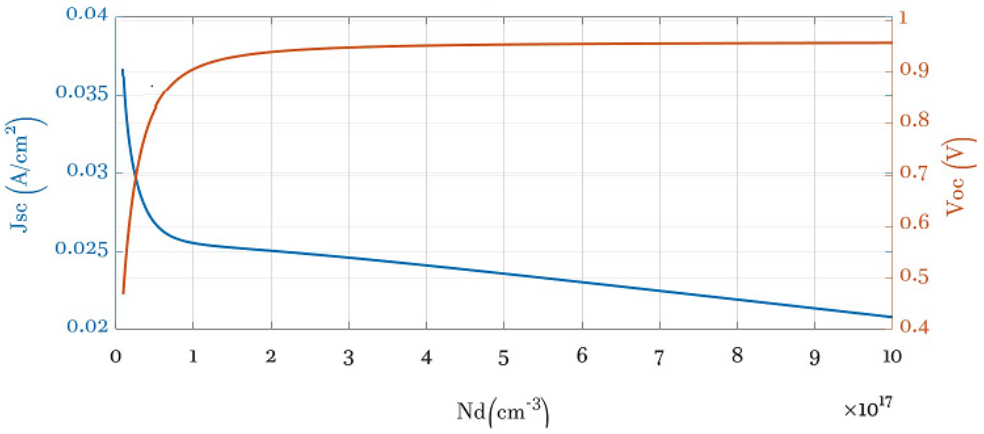

Fig. 16 Short-circuit current density (J_{sc}) and open-circuit voltage (V_{oc}) as a function of donor doping concentration (Nd)

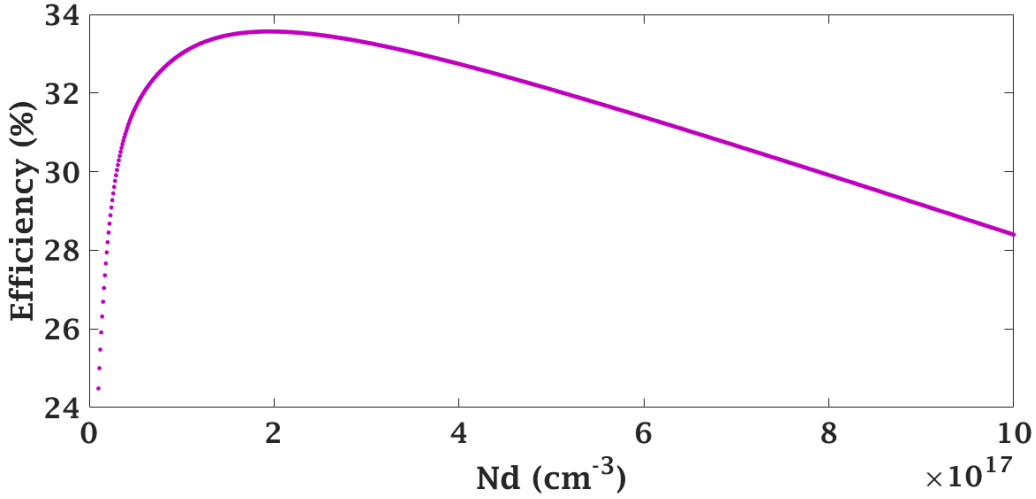

Fig. 17 Solar cell efficiency (Ƞ) as a function of donor doping concentration (Nd)

According to Fig. 16, decreasing base doping leads to an increase in short-circuit current (J_{sc}) up to a maximum value of 36.62 $mA.cm^{-2}$. This increase also causes an increase in the open-circuit voltage V_{oc} with a maximum value of 0.9569 V. Consequently the effect of these two parameters combined causes the conversion efficiency to grow to an optimum value of 33.50% obtained for $Nd = 2\ 10^{17}\ cm^{-3}$ doping and then fall with increasing base doping concentration as shown in Fig. 17. The explanations for these variations are the same as those for the effect of emitter doping.

3) *Optimum solar cell performance:* Here are the optimal values of some parameters obtained for the solar cell:

- P-layer doping concentration (acceptor) : $Na = 1.58\ 10^{18}\ cm^{-3}$
- N-layer doping concentration (donor) : $Nd = 2\ 10^{17}\ cm^{-3}$

Based on these results, we were able to determine the current-voltage (J-V) and power-voltage (P-V) characteristics of the optimized coupled solar cell under AM_1.5 illumination (0.1W/cm^2) illumination and temperature (T=300 K). The results obtained after simulation show the (J-V) and (P-V) characteristics shown in Fig. 18 and Fig. 19 respectively. The corresponding output parameters are summarized in Table III.

ISSN: 2961-6603

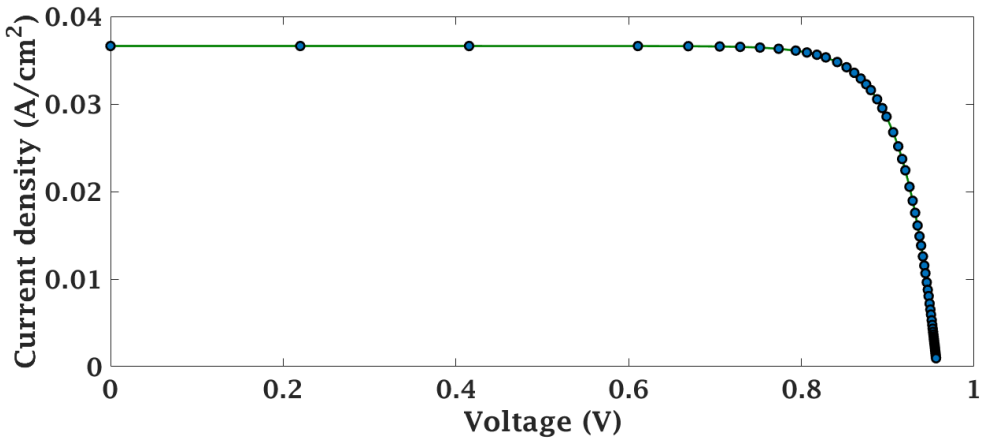

Fig. 18 Current-voltage characteristic (J-V) of the optimized coupled cell

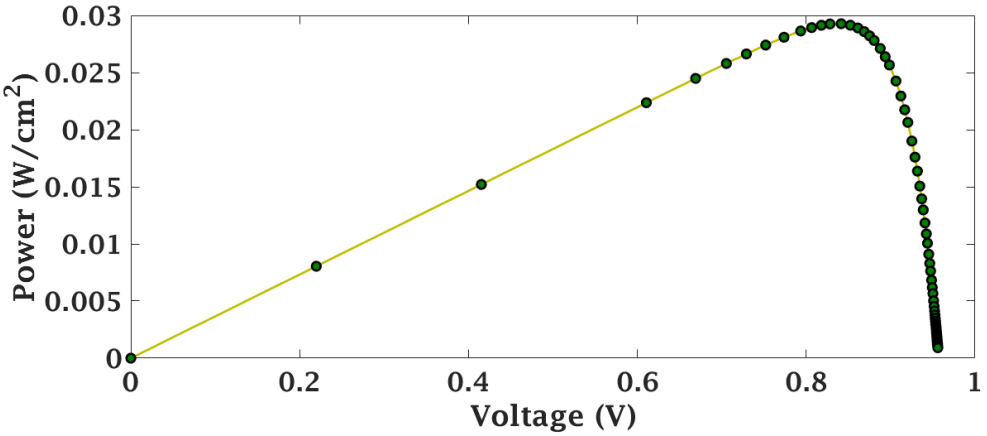

Fig. 19 Power-voltage (P-V) characteristic of the optimized coupled cell

TABLEAU III OUTPUT PARAMETERS OF THE OPTIMIZED COUPLED CELL

Parameters	**Values**
V_{co}(V)	0.9569
$J_{sc}(mA.cm^{-2})$	36.62
$P_{max}(mW.cm^{-2})$	29.27
η (%)	33.50

4) *Comparison of coupled cell, control cell and optimized coupled cell:* In order to demonstrate the performance of the model used, we will carry out a comparative study between the control cell, the coupled cell and the optimized coupled cell based on In.Ga.N. Fig. 20 and Fig. 21 show the current-voltage J(V) and power-voltage P(V) characteristics of the three cells, respectively.

ISSN: 2961-6603

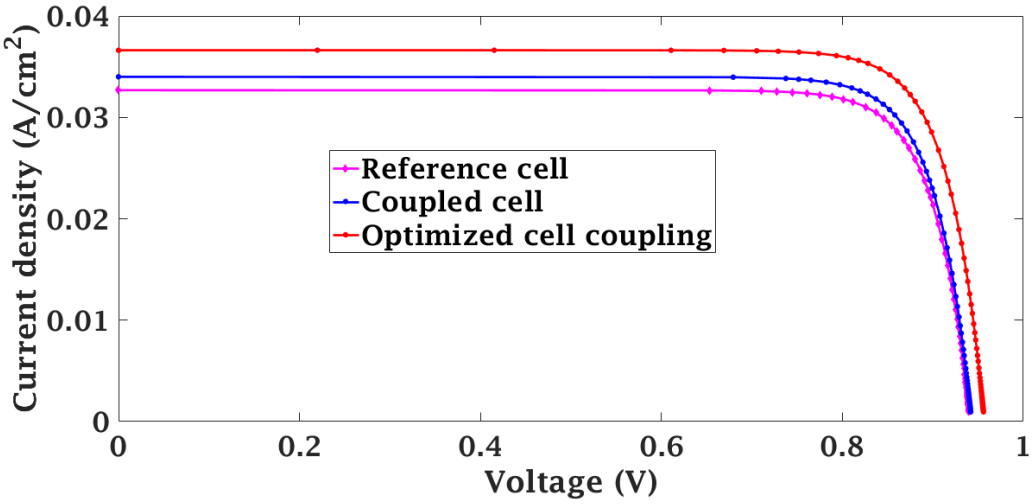

Fig. 20 Current-voltage characteristic of the three cells

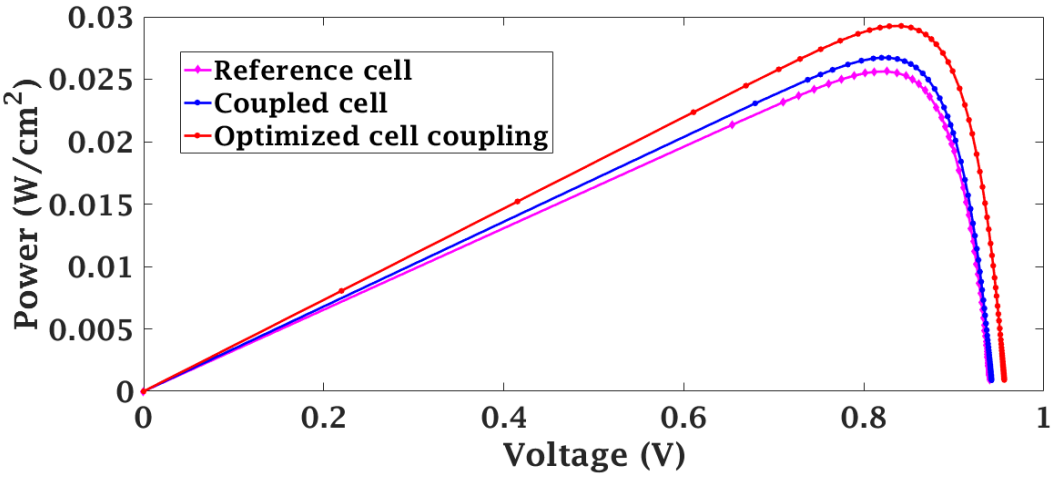

Fig. 21 Power-voltage characteristics of the three cells

From these two curves, we can see that there is an improvement in both the current-voltage characteristic J(V) and the power-voltage characteristic P(V) from the control cell to the optimized coupled cell. The photovoltaic values for these three structures are shown in Table IV below.

TABLEAU IV OUTPUT PARAMETERS OF THE THREE CELLS

	Jsc (mA/cm^2)	**Vco (V)**	**Imax (mA/cm^2)**	**Vmax (V)**	**Pmax (mW/cm^2)**	**Ƞ (%)**
Reference cell	32.67	0.94	31.53	0.81	26.51	26.50
Coupled cell	34	0.9428	32.61	0.8196	26.73	28.07
Optimized cell coupling	36.62	0.9569	34.79	0.8414	29.27	33.50

From this table, we can see that the photovoltaic quantities of the optimized coupled solar cell are significantly better than those of the coupled cell and the control cell. The improvement is most pronounced in short-circuit current (J_{sc}) and conversion efficiency (Ƞ). With the addition of the resonant structure, the short-circuit current increases from 32.68 mA. cm^{-2} to 36.62 mA. cm^{-2} and the efficiency from 26.50 % to 33.50 %. These increases

ISSN: 2961-6603

are due to the amplification of the optical field before its arrival at the "front" face of the cell, but also to the doping of the emitter and base. So the approach proposed in this work can be considered an important tool in the field of solar cell design.

VI. CONCLUSION

In this article, we have designed a resonant structure based on dielectric materials, using the complex admittance method to amplify the optical field. We then modeled an In.Ga.N-based single-junction cell under multispectral illumination in the static regime, with the aim of coupling it with the resonant structure to improve the latter's conversion efficiency. Following this coupling, a comparative study between the control cell and the coupled cell was carried out by plotting their current-voltage J(V) and power-voltage P(V) characteristics using Matlab/Simulink software; this enabled us to obtain an efficiency of 28.07% for the coupled cell versus 26.50% for the control cell.

We also carried out a parametric study of the emitter and base doping rates for this coupled cell, with the aim of obtaining an optimum structure. The results of this work have shown that the latter is obtained when the concentrations of P-layer and N-layer carriers are $1.58\,10^{18}\,\mathrm{cm}^{-3}$ et $2\,10^{17}\,\mathrm{cm}^{-3}$ respectively. Simulations carried out with this optimal structure (optimized coupled cell) under standardized conditions ($\mathrm{AM}_{1.5\mathrm{G}}$, $0.1\mathrm{W.cm}^{-2}$ et $300\mathrm{K}$) lead to a record efficiency of 33.50% compared with the control cell's 26.50%. Therefore, in view of these results, the approach adopted in this article contributes to the design of new ultra-high-efficiency solar cells.

REFERENCES

[1] RADE, "Energies renouvelables, transition énergétique et enjeux climatiques en droit africain," 2021.

[2] R. K. Kamera, "Analyse Optimisationnelle du Rendement d'un Système Solaire Photovoltaïque," vol. 6, no. 1, 2021.

[3] "Améliorer le rendement des cellules photovoltaïques : Guide Complet - Installation Panneaux Solaires." [Online]. Available: https://installation-panneaux-solaire.com/rendement-cellule-photovoltaique/. [Accessed: 27-Aug-2024].

[4] A. D. K. Kenfack and E. K. Tagne, "Behavior of a Ferromagnetic Photovoltaic Module under the Harmful Effects of an External Magnetic Field Behavior of a Ferromagnetic Photovoltaic Module under the Harmful Effects of an External Magnetic Field," no. October, 2020.

[5] S. Collin and A. Cattoni, "Les cellules solaires ultrafines," *Photoniques*, no. 102, pp. 44–48, 2020.

[6] A. Sène, C. N. Ndiaye, M. K. Mbengue, and L. Thiaw, "Nanostructured thin films coupled to single-junction solar cells: towards record efficiencies," in *Proceeding CISAI*, 2024, vol. 14, no. 5, p. 99.

[7] Michel Lequime et Claude Amra, *De l'Optique électromagnétique à l'Interférométrie Concepts et Illustrations*, EDP Scienc. 2013.

[8] A. Sène, C. N. Ndiaye, and L. Thiaw, "Absorption optimization in nano-structured optical thin films: Application to photovoltaic solar cells," in *IEEE*, 2022, pp. 1–6.

[9] A. Sène, C. N. Ndiaye, and L. Thiaw, "Efficiency improvement in photovoltaic solar cells by giant optical amplification : metallic Vs multi-dielectric coupling," *Int. J. Sci. Res. Eng. Technol.*, vol. 19, pp. 52–63, 2023.

[10] A. Mesrane, A. Mahrane, F. Rahmoune, and A. Oulebsir, "Optimal band gaps for InGaN single and double junction solar cells," *Proc. Int. Conf. Adv. Syst. Electr. Technol. IC_ASET 2017*, no. 2, pp. 335–339, 2017.

[11] A. Universit *et al.*, "Institut Fresnel Développement de systèmes de contrôle in situ des propriétés optiques de filtres interférentiels. Thèse de doctorat," 2018.

[12] D. Stojcevski, "DEVELOPPEMENT D'UN CONTROLE OPTIQUE MULTICRITERE. Application à la détermination d'indice in situ. Thèse de doctorat," 2016.

[13] S. M. Sze, *Physics of Semiconductor Devices*, Third Edit. 1981.

[14] A. Mesrane, F. Rahmoune, A. Mahrane, and A. Oulebsir, "Design and Simulation of InGaN p-n Junction Solar Cell," *Int. J. Photoenergy*, vol. 2015, p. 9, 2015.

[15] F. Bouzid and S. Ben Machiche, "Potentials of InxGa1-xN photovoltaic tandems," *J. Renew. Energies*, vol. 14, no. 1, pp. 47–56, 2023.

[16] C. A. Hernández-Gutiérrez, A. Morales-Acevedo, D. Cardona, G. Contreras-Puente, and M. López-López, "Analysis of the performance of InxGa1−xN based solar cells," *SN Appl. Sci.*, vol. 1, no. 6, 2019.

[17] L. Mousli, B. Dennai, and B. Azeddine, "MULTI-JUNCTION SOLAR CELLS (PIN / InGaN) ? ? the light intensity which decreases exponentially with thickness , so before reaching the intrinsic layer [1]:," vol. 17, no. 1, pp. 11–21, 2021.

[18] Y. Wang *et al.*, "Stabilizing heterostructures of soft perovskite semiconductors," *Science (80-.).*, vol. 365, no. 6454, pp. 687–691, 2019.

[19] Z. Z. Bandić, P. M. Bridger, E. C. Piquette, and T. C. McGill, "Minority carrier diffusion length and lifetime in GaN," *Appl. Phys. Lett.*, vol. 72, no. 24, pp. 3166–3168, 1998.

[20] F. Chen, A. N. Cartwright, H. Lu, and W. J. Schaff, "Hole transport and carrier lifetime in InN epilayers," *Appl. Phys. Lett.*, vol. 87, no. 21, pp. 1–3, 2005.

[21] P. François, K. Tagne, K. Kenfack, and A. Dimitri, "Journal of Renewable Energies," vol. 24, pp. 25–39, 2021.

ISSN: 2961-6603

[22] M. Benaicha, L. Dehimi, and N. Sengouga, “Simulation of double junction In0:46Ga0:54N/Si tandem solar cell,” *J. Semicond.*, vol. 38, no. 4, p. 6, 2017.
[23] X. Zhang *et al.*, “Simulation of In0.65Ga0.35 N single-junction solar cell,” *J. Phys. D. Appl. Phys.*, vol. 40, no. 23, pp. 7335–7338, 2007.

ISSN: 2961-6603